Journal of Sciences, Islamic Republic of Iran 20(4): 343-353 (2009) http://jsciences.ut.ac.ir
University of Tehran, ISSN 1016-1104

Cation Exchange Between Piemontite and Garnet in Piemontite-Quartz Schists from Asemi-Gawa Area of Central Shikoku, Sanbagawa Metamorphic Belt, Japan

J. Izadyar*

Department of Geology, Faculty of Science, Zanjan University, Zanjan, Islamic Republic of Iran

Received: 24 April 2009 / Revised: 14 September 2009 / Accepted: 27 October 2009

Abstract

In the Asemi-gawa area of intermediate high-pressure and low-temperature Sanbagawa metamorphic belt in central Shikoku, Japan, piemontite-quartz schists are common in which cation exchange between piemontite and garnet has been studied. Piemontite in contact with garnet usually contains two zones in which core is enriched in Mn^{3+} and surrounded by a rim rich in Fe^{3+}. Garnet is Ca-Fe-bearing spessartine and is slightly heterogeneous in which core rich in Mn is surrounded by a narrow rim poor in Mn and rich in Ca. The chemical composition of piemontite changes in contact with garnet in matrix or whenever it is included in the garnet porphyroblast. In both types of contacts, piemontite tends to be richer in Mn^{3+} and poorer in Fe^{3+} while garnet tends to be richer in Ca and Fe^{3+} and poorer in Mn^{2+}. P-T curves were calculated using piemontite-garnet equilibria and show that the chemical variation from core to rim in piemontite-garnet pair is related to increasing temperature whilst cation exchange in boundary of piemontite-garnet can be caused by decreasing temperature. Log f (O_2)-T calculations show that cores of piemontite-garnet pair have been formed under more oxidizing condition than their rims. Calculations also show cation exchange between piemontite and garnet has been occurred under more oxidizing condition than the piemontite-garnet rim.

Keywords: Spessartine garnet; Piemontite-quartz schist; Oxygene fugacity; Sanbagawa metamorphic belt; Japan

Introduction

Deep ocean sediments enriched in manganese commonly occur as protolith in high pressure metamorphic belts, for example, in Japan, USA, New Zealand [21,13,6]. Among the Mn-rich rocks, highly oxidized piemontite-quartz schists yield unusual suites of Mn-rich minerals some of which are rare or unique species [24,18,22]. Chemical variations of those minerals provide valuable information on the metamorphic P-T-t history of the host rocks and on the crystal chemistry of unusual minerals that are difficult to synthesize under low-temperature and high-pressure condition. More important, the incorporation of two

* Corresponding author, Tel.: + 98(241)5152589, Fax: +98(241)5152543, E-mail: izadyar@znu.ac.ir

transition metals (Fe and Mn) into the structure of minerals such as piemontite and garnet makes them ideal minerals for examining the relationship between crystal chemistry and mineral stability in multivalence equilibria [20]. Piemontite and garnet are two major constituent minerals of piemontite-quartz schists from the Asemi-gawa in central Shikoku, Sanbagawa metamorphic belt and thus provides the best opportunity to study cation partitioning between piemontite and spessartine under low temperature and high-pressure condition. This will be discussed in the present paper.

Geological Setting

The Sanbagawa metamorphic belt in southwest Japan is the high pressure part of the classic outer Japan pair of metamorphic belts, proposed by Miyashiro (Fig. 1) [3]. The belt is bounded to the north by the Ryoke belt, a Cretaceous low-pressure regional metamorphic belt. The two metamorphic belts are separated by a major fault, the Median Tectonic Line (MTL) (Fig. 1) [2,3,25]. The southern border of the Sanbagawa belt is placed at the southern limit of the Mikabu green stone complex and its corresponding fault. The Sanbagawa metamorphism affected a part of the Jurassic complex in which olistoliths of Carboniferous to lower Jurassic rocks such as limestone, chert and greenstone, probably formed in equatorial regions, were incorporated [3]. Sometime during the middle Cretaceous, the Jurassic complex reached a depth of about 30 km. Tectonic movement was in east-west direction or N30E on the coordinate of the pre-Japan sea Asian continent. The horizontal flow is necessary to explain the uniform metamorphic facies series, or pressure of metamorphism of the belt [3]. A little earlier than 87-85 million years ago, horizontal transport ceased and the belt started to uplift. This took place at lower temperature than the prograde metamorphism, and major mineral growth did not take place [3]. Presumably the Ryoke and Sanbagawa belts developed separately from each other, but still within the Jurassic complex on the eastern margin of the Asian continent, and were then juxtaposed by transcurrent faulting [3]. The metamorphic sequences consist mainly of pelitic, basic, psammitic and siliceous schists, associated with small amounts of ultrabasic rocks and metagabbros, and rarely with limestones [2,28]. In central Shikoku, the Sanbagawa metamorphic belt is at its widest and can be divided into four mineral zones: chlorite, garnet, albite-biotite, oligocalse-biotite zones, based on appearance of the index metamorphic minerals of pelitic schists (Fig. 1) [9,8,3]. The metamorphic temperature increases from the chlorite through the garnet and albite-biotite to oligocalse-biotite zones [9,3]. Thus the overall slope of the P-T trajectory from chlorite to the albite-biotite zone is positive (prograde path of metamorphism) but the chemical zonation of some minerals such as amphibole and garnet, suggests a retrograde path [28]. In the Asemi-gawa area the metamorphic sequences are severely sheared and folded in the boundary zone between the garnet and albite-biotite zones, and some bodies of serpentinite blocks and high-grade schists are emplaced in the sheared zone as tectonic blocks [25,2].

In the Asemi-gawa area piemontite-quartz schists are less common than pelitic and basic schists. The piemontite-quartz schists form centimeter to meter thick layers and are commonly in direct contact with pelitic and basic schists. Some of them are interbeded with the quartz-rich layers without piemontite. In the present study about 200 samples were collected from the garent zone of the Asemi-gawa area (Fig. 1).

For further details on the geology and petrology of the area the reader is referred to Banno and Sakai [3], Higashino [10] and Wallis *et al*. [28].

Analytical Procedure

Chemical analyses were obtained by a scanning electron microscope (Hitachi S550) with a Kevex energy-dispersive X-ray analytical system using the correction subroutine of Magic V program of Kevex 7000 system at Kyoto University, Japan. Standards were: pure metals for Mn, Cr and Ni; albite, wollastonite and orthoclase for Na, Ca and K; and oxides for Al, Fe, Mg, Ti. Details of the analytical procedure follow Mori and Kanehira [23] and Hirajima and Banno [11]. Back scattered electron (BSE) images were obtained using a GW-BSE detector system of the scanning electron microscope (Hitachi S530 and S550) at 20 kv and a beam current of about 1000 pA. X-ray maps were collected by Kevex advanced image software.

Because the valence states of Mn and Fe can not be determined by microprobe, they have been calculated by the following procedure. In fact, piemontite-quartz schists of the Asemi-gawa area were formed under high oxygen fugacity, such that almost all of the Fe is present as Fe^{3+} in hematite [14,17]. This conclusion is also supported by the oxidation ratio (Fe_2O_3/Fe_2O_3+FeO) in the whole rock analyses of piemontite-quartz schists which is around 100% [17]. Thus Fe was considered to be Fe^{3+} in microprobe analyses. In such high oxygen fugacity Mn is present as Mn^{3+} in the minerals such as piemontite and braunite while Mn^{2+} is mostly incorporated in spessartine [14,17]. Mn^{2+} and Mn^{3+} of piemontite were computed based on the stoichiometric

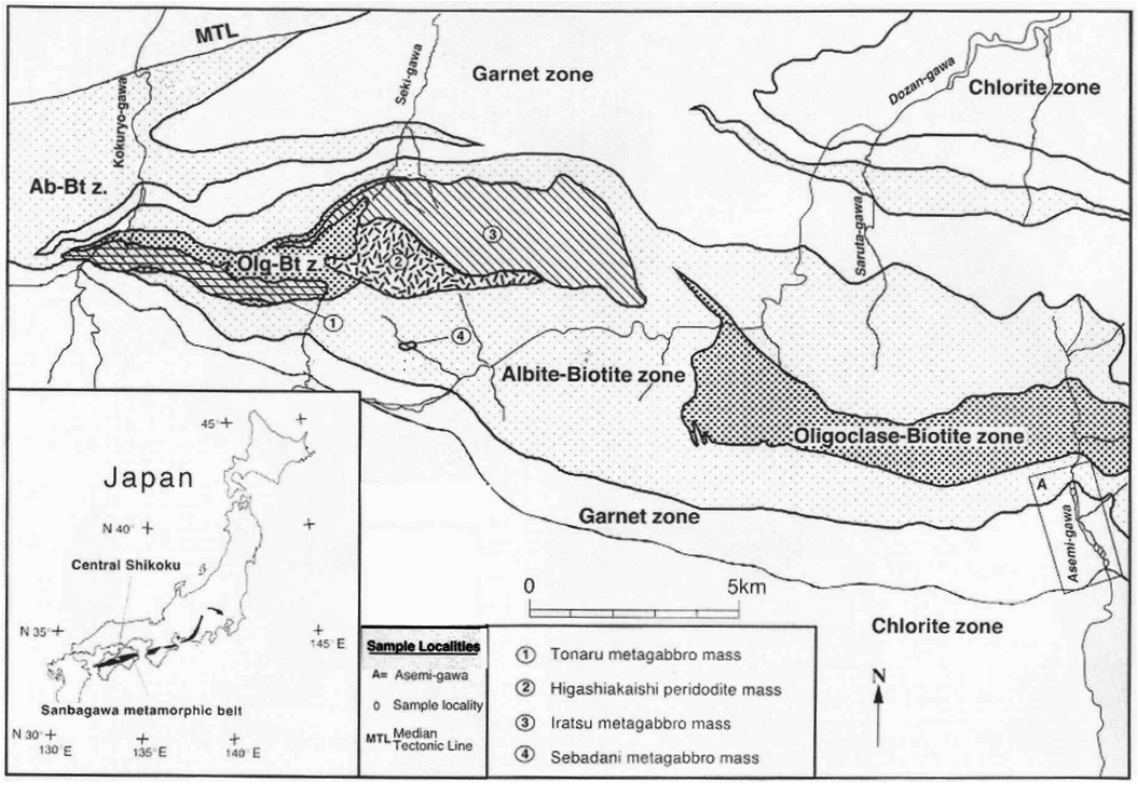

Figure 1. Metamorphic zonal map of the Sanbagawa metamorphic belt in central Shikoku (simplified from Higashino [10]) and sample localities.

formula explained in Armbruster's recommended nomenclature of epidote-group minerals [1].

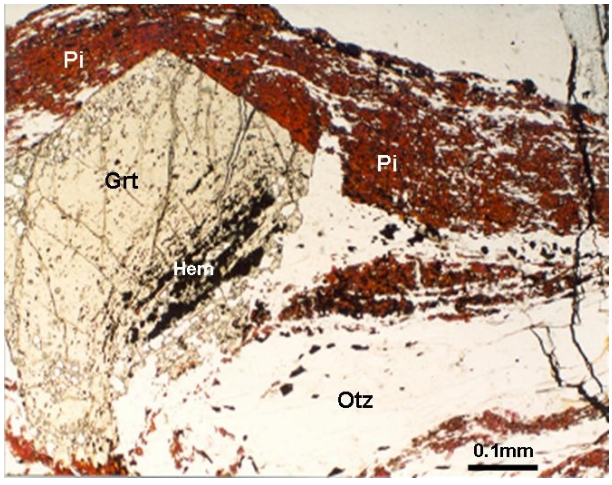

Figure 2. Photomicrograph of piemontite and garnet porphyroblast within piemontite-quartz schist from the garnet zone of Asemi-gawa (crossed nicols). Pi = piemontite, Grt = garnet, Qtz = quartz, Hem = hematite.

Petrography and Mineral Chemistry

Piemontite-quartz schists from the Asemi-gawa area commonly show compositional banding with alternating piemontite-rich and quartz-rich bands (Fig. 2). The width of the piemontite-rich bands ranges from 0.5 to 1.5 mm. They are mainly composed of piemontite, garnet, talc and hematite with subordinate amounts of quartz, phengite, chlorite, albite and braunite. The quartz-rich bands (1-2 mm thick) usually contain quartz, phengite, chlorite, albite, talc, with minor amounts of piemontite, garnet, hematite and braunite.

An epidote-group mineral is described with the generic formula $A_2M_3[T_2O_7][TO_4](O,F)(OH,O)$ [1]. The monoclinic crystal structure is composed by T_2O_7 (usually Si_2O_7) and TO_4 (usually SiO_4) units linked to two kinds of chains (parallel to the b-axis) built by edge-sharing octahedral [1,7]. One chain consists solely of edge-sharing octahedral (M2) while the other is a chain of M1 octahedra with M3 octahedra attached on alternate sides along its length. M1 and M2 cation sites are centrosymmetric while M3 is noncentrosymmetric. The framework so formed contains relatively large cavities (A sites) occupied usually by Ca in nine- or ten-

Table 1. Representative analyses of matrix piemontites and included in albite porphyroblast

	Piemontite in matrix							Piemontite in albite	
Sample No.	1205	1205	1205	1510-0	1510-0	1510-0	1510-0	1205	1205
Point No.	214	215	216	1919	2019	132	332	111	211
Core/Rim	Core	Mantle	Rim	Core	Rim	Core	Rim	-	-
SiO_2(wt%)	38.25	38.06	38.16	38.12	39.00	38.40	37.61	38.15	38.7
TiO_2	0.05	0.03	0.03	0.06	0.07	0.06	0.04	-	-
Al_2O_3	20.08	22.34	21.55	20.59	19.5	18.8	20.3	19.47	19.5
Fe_2O_3	5.71	9.44	9.43	3.82	8.34	5.10	6.11	8.78	9.23
Mn_2O_3	10.16	4.30	4.86	13.28	12.70	12.30	11.35	11.40	11.3
CaO	20.75	23.12	22.64	22.43	19.00	23.6	23.04	20.70	19.9
Total	95.00	97.29	96.67	98.35	98.60	98.4	98.45	98.51	98.70
	Si=3	Si=3	Si=3	Si=3	Si=3	Si=3	Si=3	Si=3	Si=3
Si(atoms)	3.00	3.00	3.00	3.00	3.00	3.00	3.00	3.00	3.00
Ti	0.003	0.002	0.002	0.004	0.004	0.003	0.002	-	-
Al	1.88	2.09	1.99	1.91	1.76	1.73	1.92	1.80	1.78
Fe^{3+}	0.34	0.57	0.56	0.22	0.46	0.28	0.38	0.47	0.56
Mn^{3+}	0.60	0.29	0.28	0.78	0.20	0.72	0.62	0.53	0.44
Mn^{2+}	-	-	-	0.01	0.54	-	0.05	0.13	0.21
Ca	1.74	1.95	1.90	1.90	1.57	1.97	1.97	1.75	1.64
Total	7.563	7.902	7.732	7.824	7.534	7.703	7.942	7.68	7.63
$X_{Mn^{3+}}$	0.6	0.29	0.28	0.78	0.54	0.72	0.62	0.53	0.44
$X_{Fe^{3+}}$	0.34	0.57	0.56	0.22	0.46	0.28	0.38	0.47	0.56

fold coordination [1,7]. The structure of piemontite is similar to that of epidote and other monoclinic members of the epidote group minerals in which Mn is located mainly in M3 site [1,7]. M octahedra are mainly occupied by trivalent ions such as Al, Fe^{3+}, Mn^{3+}, Cr^{3+}, V^{3+}. Divalent cations (e.g., Mg, Fe^{2+}, Mn^{2+}) may occupy M sites (preferentially M3) and M2 has a strong preference for Al whereas the occupancy of M1 and M3 depends on competing ions. The A site is divided to two types, a smaller one named A1, usually occupied by Ca or Mn^{2+} and a larger one named A2, usually occupied by Ca, Sr, Pb and REE. T_2O_7 and TO_4 are usually Si_2O_7 and SiO_4. The structural formula of piemontite was computed following Armbruster *et al*. [1]. Normalization of electron-microprobe analytical data was done on the basis of Si = 3 because normalization on the basis of $\sum$ (A+M+T) = 8 leads to Si > 3 apfu (atom per formula unit) [1]. This procedure indicates M1 and A2 site vacancies, which are most probably, field by REE elements. Mineral name of an epidote-group mineral was derivated following Armbruster *et al*. [1]. By using their recommended nomenclature, all of the analyzed minerals belong to the clinozoisite subgroup and by considering dominant cations at A1, M3 (and M2), they are piemontite or epidote. The piemontite composition is expressed by the amounts of Mn^{3+}, Fe^{3+} and Al cations on the M3 site ($X_{Fe3+} = Fe^{3+} / Al + Mn^{3+} + Fe^{3+}$, $X_{Al} = Al / Fe^{3+} + Mn^{3+} + Al$ and $X_{Mn3+} = Mn^{3+} / Al + Mn^{3+} + Fe^{3+}$) because the M3 site is mostly occupied by Mn^{3+} and Fe^{3+} in the analyzed samples.

In matrix piemontite close to the garnet usually two zones can be recognized. Piemontite of first generation (core) forms large crystal that dominates the assemblages by its modal abundance. Piemontite of second generation (rim) commonly occurs as narrow rim around core. Rim contains higher X_{Fe3+} and lower X_{Mn3+} than the core (comparing average composition of core: X_{Mn3+} = 0.75, X_{Fe3+} = 0.25 with the average composition of rim: X_{Mn3+} = 0.58, X_{Fe3+} = 0.42) (Table 1) (Figs. 3b and 4b). In the Asemi-gawa samples three generations of piemontites are also visible in matrix piemontite when it is far away from garnet. In this case, the core with average composition of X_{Mn3+}=0.60 and X_{Fe3+}=0.34 is surrounded by a mantle with composition of X_{Mn3+}=0.29 and X_{Fe3+}=0.57. The mantle, in turn, is

surrounded by a rim characterized by X_{Mn}^{3+}=0.28 and X_{Fe}^{3+}= 0.56 (Table 1). Also piemontite occurs as inclusion in albie porphyroblasts and its chemical composition is X_{Mn}^{3+}=0.48 and X_{Fe}^{3+}=0.52 (Table 1).

The unit cell of garnet contains eight $X_3Y_2Z_3O_{12}$ formula units. The structure consists of alternating ZO_4 tetrahedra and YO_6 octahedra which share corners to form a three-dimentional network. Within this there are cavities that can be described as distored cubes of eight oxgens which contain the X ions [7]. Divalent cations such as Ca, Mg, Fe and Mn commonly occupy X sites. The Y site usually occupied by Al, Fe^{3+} and Cr. Al with Si dominant tetrahedral position [7]. The garnet composition is expressed by the amounts of Mn^{2+}, Ca and Mg on X sites and Fe^{3+} and Al contents on Y sites ($X_{Mn}^{2+} = Mn^{2+}/ Mn^{2+} + Ca + Mg$; $X_{Ca} = Ca / Mn^{2+} + Ca + Mg$; $X_{Mg} = Mg / Mn^{2+} + Ca + Mg$; $X_{Fe}^{3+} = Fe^{3+} / Fe^{3+} + Al$; $X_{Al} = Al / Fe^{3+} + Al$).

Porphyroblasts of garnets occur in both piemontite- and quartz-rich bands. Garnet in piemontite-rich bands is euhedral and its size ranges from 1 to 3 mm. This type of garnet is poikiloblastic containing many inclusions of piemontite, quartz, hematite, braunite, phengite and amphibole. Chemically, these garnets are Ca-Fe-bearing spessartine (X_{Mn}^{2+}=0.85, X_{Ca}=0.13, X_{Fe}^{3+}=0.05, X_{Mg}=0.02) and are slightly heterogenous in which its rim becomes poorer in Mn and Ca and richer in Mg (X_{Mn}^{2+}=0.82, X_{Ca}=0.12, X_{Fe}^{3+}=0.05, X_{Mg}=0.04) (Table 2) (Figs. 3a and 4a). The second type of garnet occurs in quartz-rich bands and includes only small amounts of hematite, piemontite and braunite and its size ranges from 0.5 to 1.5 mm. It is also Ca-Fe- bearing spessartine (X_{Mn}^{2+}=0.84, X_{Ca}=0.14, X_{Fe}^{3+}=0.05, X_{Mg}=0.02) and chemically is slightly zoned in which from core to rim X_{Mn}^{2+} and X_{Ca} decrease while X_{Mg} increases (X_{Mn}^{2+} = 0.82, X_{Ca} = 0.13, X_{Fe}^{3+} = 0.05, X_{Mg} = 0.03) (Table 2) (Figs. 3a and 4a).

Braunite occurs as aggregates of subhedral crystals, which is intimately intergrown with quartz, or it is randomly interspersed as small particle among coarser-grained main constituents. Average structural formula of braunite is: $(Ca_{0.03}Mn^{2+}_{0.6}\ Mg_{0.01})\ (Mn^{3+}_{5.07}\ Fe^{3+}_{0.93})\ SiO_{12}$.

Talc occurs as tabular aggregates or as an intercalation with phengite or chlorite and is very close to the ideal Mg end-member (Table 3).

Chlorite occurs in contact with phengite and talc and is commonly combined with piemontite, garnet, braunite and hematite. Representative chemical composition of the chlorite is tabulated in Table 3. The average composition of the analyzed chlorite is close to the ideal clinochlore end-member.

Phengite is a major phyllosilicates in the studied

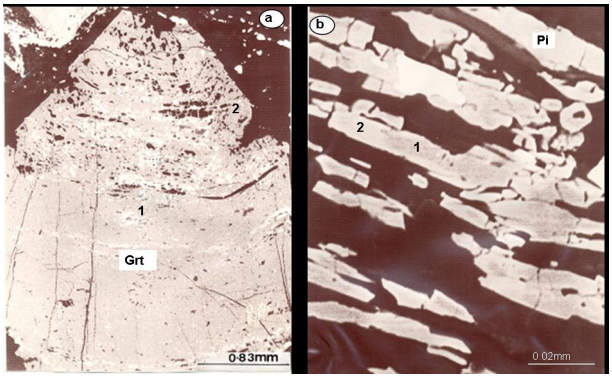

Figure 3. a) Back scattered electron image of the garnet showing two zones. The major part of garnet is homogeneous core (1) with enrichment in Mn^{3+} and number 2 is narrow rim surrounding core with slightly depletion in Mn^{3+}. b) Back scattered electron image of the matrix piemontite showing two zones: 1= core with enrichment in Mn^{3+} and 2= rim with enrichment in Fe^{3+} and depletion in Mn^{3+}. Pi = piemontite, Grt = garnet.

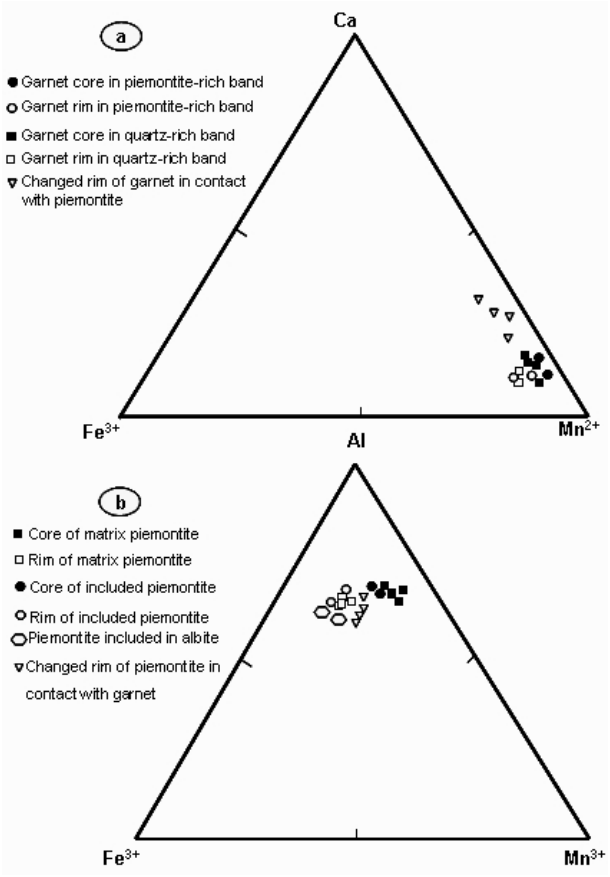

Figure 4. a) Chemical compositions and compositional variations of garnets in Ca-Fe^{3+}-Mn^{2+} triangular diagram. b) Chemical compositions and compositional variations of piemontites in Al-Fe^{3+}-Mn^{3+} triangular diagram.

Table 2. Representative analyses of garnets in piemontite- and quartz-rich bands. Also analyses of garnets at contact with piemontite are tabulated

	Garnet in piemontite-rich band				**Garnet in quartz-rich band**				**Changed rim of garnet**			
Sample No.	1510-0	1510-0	1510-0	1510-0	1510-0	1510-0	1510-0	1510-0	1510-0	1510-0	1510-0	1510-0
Point No.	27	32	43	34c	130	230	530	531	1619	4619	1419	4419
Core/Rim	Core	Rim	Core	Rim	Core	Rim	Core	Rim	-	-	-	-
SiO_2(wt%)	37.39	37.05	37.2	37.45	37.46	37.63	37.24	37.62	37.33	37.98	37.92	38.20
TiO_2	0.23	0.24	0.28	0.28	0.25	0.27	0.41	0.30	0.14	0.15	0.09	0.08
Al_2O_3	19.58	19.64	19.41	19.86	19.62	19.68	18.76	19.67	19.67	19.24	20.31	19.68
Fe_2O_3	1.74	1.80	1.60	2.20	1.73	1.87	1.89	2.41	2.65	3.05	3.40	3.79
MnO	36.92	36.54	36.38	35.01	35.71	35.55	35.73	34.75	30.43	32.31	30.14	26.90
MgO	0.71	0.86	0.42	0.90	0.57	0.76	0.52	0.72	0.77	0.50	0.72	0.65
CaO	4.08	4.79	4.97	4.05	4.47	4.20	5.12	4.37	8.95	7.04	9.30	11.06
Total	100.6	100.9	100.20	99.75	99.80	99.9	99.67	99.84	99.94	100.2	101.8	100.3
No.Ox.	12	12	12	12	12	12	12	12	12	12	12	12
Si(atoms)	3.04	3.00	3.03	3.06	3.04	3.03	3.07	3.06	3.00	3.00	2.98	3.03
Ti	0.01	0.01	0.01	0.01	0.01	0.01	0.02	0.02	0.009	0.009	0.004	0.005
Al	1.86	1.86	1.86	1.88	1.87	1.86	1.78	1.85	1.86	1.83	1.88	1.84
Fe^{3+}	0.09	0.09	0.10	0.10	0.10	0.11	0.10	0.10	0.09	0.19	0.36	0.22
Mn^{2+}	2.55	2.49	2.49	2.42	2.46	2.44	2.48	2.43	2.10	2.18	1.95	1.81
Mg	0.08	0.09	0.05	0.10	0.07	0.1	0.05	0.10	0.09	0.05	0.08	0.07
Ca	0.34	0.39	0.44	0.35	0.38	0.34	0.45	0.39	0.8	0.63	0.75	0.94
Total	7.97	7.93	7.98	7.92	7.95	7.90	7.95	7.95	7.95	7.90	7.96	7.91
$X_{Mn^{2+}}$	0.86	0.83	0.84	0.82	0.85	0.84	0.83	0.81	0.70	0.76	0.70	0.64
$X_{Fe^{3+}}$	0.05	0.05	0.05	0.05	0.05	0.05	0.05	0.04	0.05	0.10	0.08	0.08
X_{Ca}	0.11	0.13	0.15	0.12	0.13	0.13	0.15	0.13	0.27	0.22	0.27	0.33
X_{Mg}	0.03	0.03	0.02	0.04	0.02	0.03	0.02	0.03	0.03	0.02	0.03	0.02

samples and occurs in the matrix and as an inclusion in albite porphyroblast (Table 3).

Phlogopite can only found at the margin of the phengite and its chemical composition is tabulated in Table 3.

Colorless amphibole commonly occurs as inclusion in albite and garnet porphyroblasts and its composition corresponds to crosstie (Table 3).

Albite occurs as porphyroblast and commonly contains abundant inclusions of piemontite, hematite, phengite, colorless amphibole and quartz. Its chemical composition is close to the ideal albite and is homogenous.

Hematite occurs in the matrix and as inclusion in albite and garnet and its average composition is: $(Fe_{1.90}Mn_{0.08}Ti_{0.01})O_3$.

For further details on the chemical compositions of the piemontite-quartz schists see Izadyar *et al.* [15], Izadyar [14], Izadyar *et al.*[16] and Izadyar [17].

Cation Exchange between Piemontite and Garnet

The chemical composition of piemontite changes whenever occurs as inclusion in garnet or in contact to it in matrix. The change was observed in their rims in a very limited area about 10 μm away from their boundary (Figs. 5a and b). At the contact, piemontite tends to be on average richer in Mn^{3+} ($X_{Mn^{3+}} = 0.62$) and poorer in Fe^{3+} ($X_{Fe^{3+}} = 0.38$) as compared to inner part ($X_{Mn^{3+}} = 0.52$, $X_{Fe^{3+}} = 0.48$) (Table 4) (Figs. 4b and 6). The zoning at the edges of the garnet is steep with Ca and Fe^{3+} increasing while Mn^{2+} decreases ($X_{Mn^{2+}} = 0.70$, $X_{Fe^{3+}} = 0.08$, $X_{Ca} = 0.27$) comparing to the inner part ($X_{Mn^{2+}} = 0.83$, $X_{Fe^{3+}} = 0.05$, $X_{Ca} = 0.13$) (Table 2) (Figs. 4a and 6). Of particular note here is the lack of significant zoning in the interior of the crystal. Garnets displaying this type of pattern in their zoning are interpreted to have been almost homogeneous and subsequent

Table 3. Representative analyses of phengite, chlorite, crosstie, talc and phlogopite

Mineral name	Phengite	Chlorite	Crossite	Talc	Phlogopite
Sample No.	1205	1205	1205	1510	1510
PointNo.	115	113	29	156	1414
SiO_2	48.26	30.05	59.22	63.15	46.88
TiO_2	0.58	0.09	-	-	-
Al_2O_3	26.92	20.43	7.47	-	10.88
Fe_2O_3	-	-	7.28	-	0.77
Mn_2O_3	-	-	0.78	-	-
FeO	3.47	0.67	-	0.07	-
MnO	0.11	0.08	-	0.33	1.21
MgO	3.39	32.65	14.35	30.96	24.57
CaO	-	0.07	0.48	-	-
Na_2O	1.08	-	7.01	-	-
K_2O	9.96	-	0.04	-	10.17
Total	93.77	84.04	96.63	94.51	94.48
	O=22	O=28	O=23	O=22	O=22
Si	6.66	5.80	8.03	8.00	6.53
AlIV	1.28	2.19	-	-	1.47
AlVI	3.05	2.45	1.19	-	0.36
Ti	0.06	0.01	-	-	-
Fe_{3+}	-	-	0.74	-	0.08
Mn_{3+}	-	-	0.08	-	-
Fe_{2+}	0.42	0.10	-	0.007	-
Mn_{2+}	0.008	0.01	-	0.03	0.14
Mg	0.66	9.28	2.90	5.90	5.10
Ca	-	0.01	0.07	-	-
Na	0.28	-	1.84	-	-
K	1.66	-	0.006	-	1.80
Total	14.07	19.85	14.86	13.95	15.44

diffusion at the rims modified the composition to the pattern observed [27]. These relations show diffusion of Mn from X site of garnet to M3 site of piemontite and inversely Fe from M3 site of piemontite to Y site of garnet and Ca from A site of piemontite to X site of garnet. Also excess of Mn as Mn^{2+} substitutes on A site of piemontite in order to maintain local charge balance.

Results and Discussion

The relation between garnet and piemontite in the piemontite-quartz schists of Asemi-gawa may be discussed by using simplified reaction of piemontite = garnet + fluid. Keskinen and liou [19] determined the loci of the reaction in log $f(O_2)$-T space to very oxidizing conditions. Their experiments show that the stability of piemontite is strongly controlled by the $f(O_2)$ and also considered that introduction of Fe^{3+} in piemontite will extend its stability towards higher temperature and lower oxygen fugacity. Brown *et al*. [4] calculated $f(O_2)$ values for manganese-rich metamorphic rocks using piemontite-garnet reaction. Their calculation indicates that the reaction is very sensitive to the oxidation state and likely represents a viable oxybarometer.

The complex garnet composition in the reaction can be separated into the end-members of grossular and spessartine for which thermodynamic properties are known:

$$12Ca_2MnAl_2Si_3O_{12}(OH) = 8Ca_2Al_2Si_3O_{12} + 4Mn_3Al_2Si_3O_{12} + 6H_2O + 3O_2$$

piemontite *grossular* *spessartine* *fluid*

For this reaction, it can be written:

$\Delta G_{(P,T)} = \Delta G_T + \Delta Vs\Delta P + \int_1^P V_{H2O} + RT\ Ln\ (fO_2)^3 (a_{grossular})^8 (a_{spessartine})^4 / (a_{piemontite})^{12}$

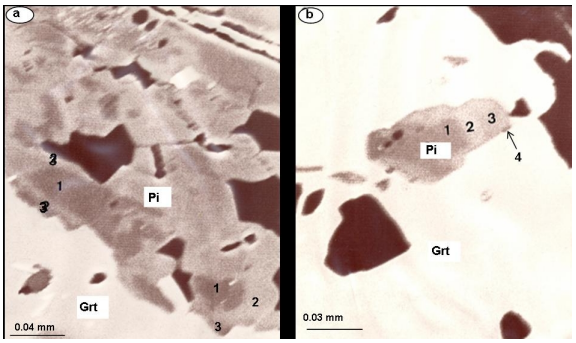

Figure 5. a) Back scattered electron image of piemontite-garnet contact in matrix. 1 = core of piemontite with enrichment in Mn^{3+}, 2= rim of piemontite with depletion in Mn^{3+} and enrichment in Fe^{3+}, 3= boundary of piemontite and garnet in which Mn^{3+} of piemontite increases and its Fe^{3+} and Ca decrease while in garnet edge (approximately 3μm) Mn^{2+} decreases and Fe^{3+} and Ca increase. b) Back scattered electron image of included piemontite in garnet porphyroblast. 1= core of piemontite with enrichment in Mn^{3+}, 2= rim of piemontite with depletion in Mn^{3+} and enrichment in Fe^{3+}, 3= changed rim of piemontite with enrichment in Mn^{3+} and depletion in Fe^{3+}, 4= narrow changed rim of garnet (approximately 3μm) in which Mn^{2+} decreases while Fe^{3+} and Ca increase. Pi = piemontite, Grt = garnet.

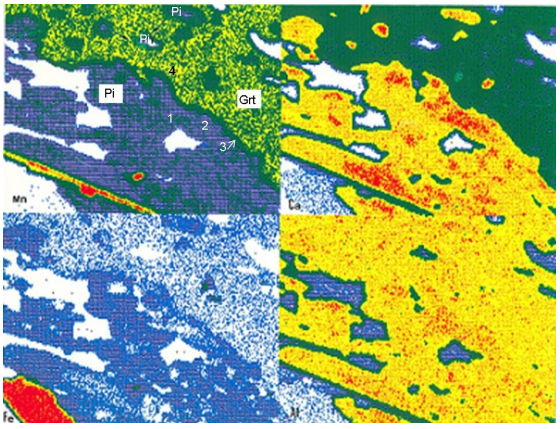

Figure 6. Map of X-ray intensity distribution for Mn, Ca, Fe and Al for the piemontite-garnet contact (both included in garnet porphyroblast and in matrix). 1= core of piemontite with enrichment in Mn^{3+}, 2= rim of piemontite with depletion in Mn^{3+}, 3= changed rim of piemontite with enrichment in Mn^{3+}, 4= changed rim of garnet with depletion in Mn^{2+}. Pi = piemontite, Grt = garnet. Relative intensities increase in the order blue-green-yellow-red.

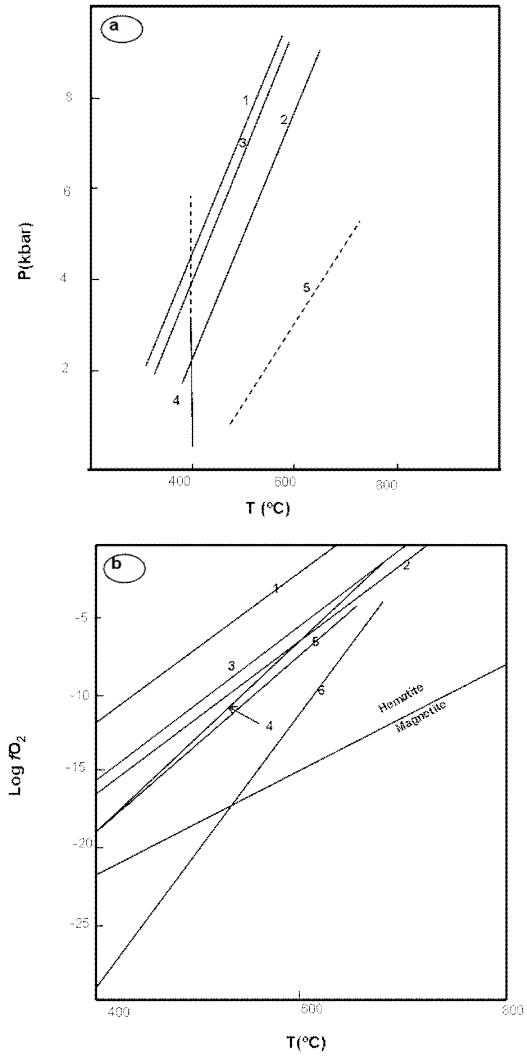

Figure 7. a)P-T plot calculated using the piemontite-garnet reaction for core (1), rim (2) and contact of piemontite with garnet (3) for copper-cuperite buffer. Curves 4 and 5 were calculated by Keskinen and Liou [20] for %33 and %17 piemontite respectively for copper-cuperite buffer. b) Log $f(O_2)$-T plot calculated using the piemontite-garnet oxybarometer between 400 and 800 °C temperature for core (1), rim (2) and contact of piemontite with garnet (3). Log $f(O_2)$-T curves obtained by Brown *et al*. (4) [4], Keskinen and Liou (5) [19] and Singer (6) [26] are also shown for comparison. The hematite-magnetite buffer line (7) is adapted from Brown *et al*. [4].

Where ΔG_T is the Gibbs free energy and ΔVs is the change in volume of the solids between reactants and products. This equation allows calculation of $f(O_2)$. The calculations in this study were done at temperatures between 400 and 800°C. The $f(O_2)$ is fixed at a given P and T when the activities of grossular, spessartine and piemontite are known. The activities of the garnet were

Table 4. Representative analyses of matrix piemontites and included piemontite in garnet porphyroblast. Rim 2 is the analysis of piemontite at contact with garnet

	Matrix piemontite at contact to garnet						**Included piemontite in garnet**					
Sample No.	1510-0	1510-0	1510-0	1510-0	1510-0	1510-0	1510-0	1510-0	1510-0	1510-0	1510-0	1510-0
Point No.	3419	3319	3519	832	732	932	719	819	1019	2819	3019	3119
Core/Rim	Core	Rim 1	Rim 2	Core	Rim 1	Rim 2	Core	Rim 1	Rim 2	Core	Rim 1	Rim 2
SiO_2(wt%)	37.94	37.34	37.69	37.77	37.68	37.09	37.82	37.23	37.71	37.19	37.45	37.40
TiO_2	0.04	0.07	0.06	0.04	0.05	0.11	0.06	0.09	0.05	0.08	0.07	0.12
Al_2O_3	20.15	20.19	20.24	20.41	19.90	20.63	20.16	20.06	20.04	20.44	19.87	19.43
Fe_2O_3	5.88	8.38	7.08	5.17	8.88	6.38	4.88	8.57	7.10	6.37	7.19	7.15
Mn_2O_3	11.20	10.88	13.58	12.92	11.39	14.07	11.64	10.71	14.61	11.62	11.19	13.49
CaO	23.11	21.45	19.29	22.45	20.69	19.94	22.89	21.24	19.16	23.15	21.83	20.07
Total	98.10	98.31	97.94	98.70	98.59	98.20	97.45	97.90	98.00	98.80	97.60	97.60
	Si=3	Si=3	Si=3	Si=3	Si=3	Si=3	Si=3	Si=3	Si=3	Si=3	Si=3	Si=3
Si(atoms)	3.00	3.00	3.00	3.00	3.00	3.00	3.00	3.00	3.00	3.00	3.00	3.00
Ti	0.002	0.004	0.003	0.002	0.003	0.005	0.003	0.004	0.003	0.004	0.004	0.009
Al	1.90	1.93	1.90	1.90	1.86	1.94	1.90	1.94	1.80	1.94	1.84	1.84
Fe_{3+}	0.28	0.48	0.38	0.28	0.47	0.29	0.29	0.48	0.38	0.39	0.39	0.39
Mn_{3+}	0.66	0.52	0.62	0.72	0.50	0.68	0.67	0.52	0.64	0.61	0.61	0.61
Mn_{2+}	-	0.15	0.14	0.04	0.16	-	-	0.15	0.24	0.07	0.07	0.16
Ca	1.95	1.84	1.62	1.90	1.76	1.70	1.95	1.89	1.62	1.98	1.88	1.74
Total	7.792	7.924	7.663	7.842	7.753	7.615	7.813	7.984	7.683	7.994	7.794	7.749
$X_{Mn^{3+}}$	0.66	0.52	0.62	0.72	0.50	0.68	0.67	0.52	0.64	0.61	0.61	0.61
$X_{Fe^{3+}}$	0.28	0.48	0.38	0.28	0.47	0.29	0.29	0.48	0.38	0.39	0.39	0.39

calculated using AX program of Holland and Powell [12]. The Gibbs free energy and entropy data for grossular and spessartine are from Holland and Powell [12]. The activity of piemontite was taken to be the mol fraction of Mn^{3+} in the M3 site using ideal model. The Gibbs free energy and entropy data for piemontite are from Singer [26]. Since piemontite requires H_2O-rich conditions, the water has been approximated as pure. Thermodynamic properties of water were taken from Burnham *et al*. [5].

The P-T slope of the reaction is nearly independent of pressure, especially for the copper-cuprite buffer. This is consistent with a calculated change in volume for the reaction, which, when combined with the positive change in entropy for a dehydration reaction, suggests a vertical to slightly positive pressure-temperature slope for the piemontite breakdown reaction. The effect of pressure on dehydration temperature is apparently very minor in comparison to the effect of oxygen fugacity.

Figure 7a shows the P-T curves calculated using piemontite-garnet reaction for average chemical compositions of piemontite-garnet pair at their cores and rims and their contact for fixed oxygen fugacity of copper-cuprite buffer. For comparison, P-T curves obtained by Keskinen and Liou [20] are also shown. Even though, the obtained P-T curves of the reaction take place over a narrow divariant P-T region, but it can be seen that P-T curve of rim composition occurred at higher temperature than the core while P-T curves of piemontite-garnet reaction using their contact compositions is located at the lower temperature than the rim composition curve. The obtained results fit well with the experimental results of Keskinen and Liou [19,20]. Therefore, the chemical variation from core to rim in piemontite-garnet pair is related to increasing temperature whilst the cation exchange in boundary of piemontite-garnet can be caused by decreasing temperature.

The very close P-T stability curves suggest that oxygen fugacity may be more important control on piemontite-garnet reaction than temperature. In fact, the presence of different valence states for Mn and Fe in the piemontite and garnet makes it necessary to control

oxygen fugacity. To investigate the $f(O)_2$ effect, an oxygen barometer has been developed using mentioned garnet-piemontite equilibria. The calculations were done at temperature between 400 and 800ºC. Figure 7b shows the log $f(O_2)$-T curves calculated using the piemontite-garnet oxybarometer for Asemi-gawa between 400 and 800ºC temperature. For comparison log $f(O_2)$ curves obtained by Brown *et al*. [4], Singer [26] and Keskinen and Liou [19] for the piemontite-garnet oxybarometer are also shown. The $f(O_2)$ calculation was conducted over the temperature range of 400-800°C at 8.5 kbar for Asemi-gawa samples and yielded $f(O_2)$ values approximately ten log $f(O_2)$ units more oxidizing than hematite-magnetite buffer for core composition. The piemontite-garnet reaction for rim composition shifts approximately three log $f(O_2)$ units lower relative to the core composition curve. The obtained results fit well with the experimental results of Keskinen and Liou [19,20] that by increasing $f(O_2)$, the $X_{Mn^{3+}}$ of piemontite also increases. Calculation of the $f(O_2)$ for the chemical compositions of garnet and piemontite at their contact imply oxidizing condition for cation exchange between garnet and piemontite. Log $f(O_2)$-T curve obtained for piemontite-garnet contact composition shifts approximately one log units higher relative to the rim composition curve. The interpretation for the chemical changes at piemontite-garnet contact is that an initially equilibrium compositions of piemontite and garnet were modified by diffusion of Fe, Mn and Ca in the vicinity of piemontite and garnet which they were reacting. Diffusion occurs because changes in the physical conditions experienced by a rock cause reactions to proceed, which change the equilibrium compositions on their rims of the crystals. With decreasing temperature and increasing oxygen fugacity the diffusion will proceed, causing Ca and Fe^{3+} at the rim of garnet to increase while Mn^{3+} at the rim of piemontite increases.

Acknowledgments

The Ministry of Education of Japan supported this study; this support is gratefully acknowledged.

References

1. Armbruster T., Bonazzi P., Akasaka M., Bermanec V., Chopin C., Giere R., Heuss- Assbichler S., Liebscher A., Menchetti S., Pan Y. and Pasero M. Recommended nomenclature of epidote-group minerals. *European Journal of Mineralogy*, **18**: 551-567 (2006).
2. Banno S., Sakai C. and Higashino T. Pressure-temperature trajectory of the Sanbagawa metamorphism deduced from garnet zoning. *Lithos*, **19**: 51-63 (1986).
3. Banno S., Sakai C. Geology and metamorphic evolution of the Sanbagawa metamorphic belt, Japan. *Geoogical Society Special Publication*, **43**: 519-532 (1989).
4. Brown P., Essene E.J. and Peacor D.R. The mineralogy and petrology of manganese-rich rocks from St. Marcel, Piedmont, Italy. *Contributions to Mineralogy and Petrology*, **67**: 227-232 (1978).
5. Burnham C.W., Holloway J.R. and Davis N.F. Thermodynamic properties of water to 1000ºC and 10000bars. *Memorial of Geological Society of America Special Papper*, 132 (1969).
6. Coombs D.S., Dowse M., Grapes R., Kawachi Y. and Roser B. Geochemistry and origin of piemontite-bearing and associated manganiferous schists from Arrow Junction, western Otago, New Zealand. *Chemical Geology*, **48**: 57-78(1985).
7. Deer W.A., Howie R.A. and Zussman J. *An introduction to the rock forming minerals*. Longman, London, 549 p.(1992).
8. Enami M. Oligoclase-biotite zone of the Sanbagawa metamorphic terrain in the Besshi district, central Shikoku, Japan. *Journal of Geological Society of Japan*, **88**: 887-900 (1982).
9. Higashini T. Biotite zone of Sanbagawa metamorphic terrain in the Siragayama area, central Shikoku, Japan. *Journal of Geological Society of Japan*, **81**: 653-670 (1975).
10. Higashino T. The higher grade metamorphic zonation of the Sanbagawa metamorphic belt in central Shikoku, Japan. *Journal of Metamorphic Geology*, **8**: 413-423 (1990).
11. Hirajima T. and Banno S. Electron-microprobe analysis of rock forming minerals with Kevex-delta IV (Quantum detector). *Hitachi Scientific Instrument News*, **34**: 1118-1134 (1991).
12. Holland T.J.B. and Powell R. An internally consistent thermodynamic data set for phases of petrological interest. *Journal of Metamorphic Geology*, **16**: 309-43 (1998).
13. Huebner J.S., Flohr M.J.K. and Grossman J.N. Chemical fluxes and origin of a manganese carbonate-oxide-silicate deposit in bedded chert. *Chemical Geology*, **100**: 93-118 (1992).
14. Izadyar J. Chemical composition of piemontites and reaction relations of piemontite and spessartine in piemontite-quartz schists of central Shikoku, Sanbagawa metamorphic belt,Japan. *Schweiz. Mineral. Petrogr. Mitt.*, **80**: 199-210 (2000).
15. Izadyar J., Hirajima T. and Nakamura D. Talc-phengite assemblage in piemontite-quartz schist of the Sanbagawa metamorphic belt, central Shikoku, Japan. *The Island Arc*, **9**: 145-156 (2000).
16. Izadyar J., Tomita K. and Shinjoe H. Geochemistry and origin of piemontite-quartz schists in the Sanbagawa Metamorphic Belt, central Shikoku, Japan. *Journal of Asian Earth Sciences*, **21**: 711-730.
17. Izadyar J. Multiple stages of piemontite formation in piemontite-quartz schists of the Sanbagawa metamorphic belt in central Shikoku, Japan. *GeoActa*, **6**: 57-68 (2007).
18. Kawachi Y., Grapes R. H., Coombs D.S. and Dowse M. Mineralogy and petrology of a piemontite-bearing schist, western Otago, New Zealand. *Journal of Metamorphic*

Geology, **1**: 353-372 (1983).
19. Keskinen M. and Liou J.G. Synthesis and stability relations of Mn-Al piemontite, $Ca_2MnAl_2Si_3O_{12}(OH)$. *American Mineralogist*, **64**: 317-328 (1979).
20. Keskinen M. and Liou J.G. Stability relations of Mn-Fe-Al piemontite. *Journal of Metamorphic Geology*, **5**: 495-507 (1987).
21. Matsumoto R. Origin of manganese nodules in the Jurassic siliceous rocks of Inuyama district, central Japan. In: Hein J.R. (Ed.), *Siliceous sedimantry Rocks-hosted Ores and Petroleum.* Van Nostrand Reinhold, New York, pp. 181-205 (1987).
22. Minakawa T. Study on characteristic mineral assemblages and formation process of metamorphosed manganese ore deposit in bedded chert. *Chemical Geology*, **100**: 93-118 (1992).
23. Mori K. and Kanehira K. X-ray energy spectometery for electron probe analysis. *Journal of Geological Society of Japan*, **90**: 271-285 (1984).
24. Reinecke T. Crystal chemistry and reaction relation of piemontites and thulites from highly oxidized low grade metamorphic rocks at Vitali, Andros Islands, Greece. *Contributions to Mineralogy and Petrology*, **93**: 56- 76 (1986).
25. Sakai C. Metamorphism and deformation of the Sanbagawa metamorphic terrain, central Shikoku, PhD *Thesis*, Kyoto University, 246p. (1985).
26. Singer D. Highly oxidized rocks from the San Gorgonio Pass, California; petrology and thermodynamic calculations. Senior Honors *Thesis*, University of Michigan (2002).
27. Spear F.S. *Metamorphic phase equilibria and pressure-temperature-time paths.* Mineralogical Society of America, Washington D.C., 799p. (1993).
28. Wallis S.R., Banno S. and Radvance M. Kinematic, structure and relationship to metamorphism of east-west flow in the Sanbagawa belt, Southwest Japan. *The Island Arc*, **1**: 176-185 (1992).